

Microwave-assisted photocatalysis of neurotoxin compounds using metal oxides quantum dots/nanosheets composites: Photocorrosion inhibition, reusability and antibacterial activity studies

Ali Fakhri^{a,*}, Mona Azad^b, Leila Fatolahi^c, Shiva Tahami^d

^a Young Researchers and Elites Club, Science and Research Branch, Islamic Azad University, Tehran, Iran

^b Department of Chemical Engineering, North Tehran Branch, Islamic Azad University, Tehran, Iran

^c Department of Chemistry, Payame Noor University (PNU), Iran

^d Department of Biology, Karaj Branch, Islamic Azad University, Karaj, Iran

ARTICLE INFO

Keywords:

Quantum dots
Nanosheets
Optical properties
Photocorrosion
Antibacterial activity
Photocatalysis

ABSTRACT

Water pollution caused by different pollutants is one of the challenging tasks for the scientific community. We have prepared and characterized a material for removal of pollutant compounds. ZnO quantum dots decorated CuO nanosheets and TiO₂ quantum dots decorated WO₃ nanosheets composites have been prepared using a hydrothermal method. The as synthesized catalysts were characterized by various techniques. The crystallite sizes of CuO NSs and WO₃ NSs were to be obtained 12.5 and 13.25 nm and when doped with ZnO and TiO₂ size reduces to 3.2 and 3.9 nm, respectively. The energy band gap of the CuO NSs, WO₃ NSs, ZnO QDs/CuO NSs and TiO₂ QDs/WO₃ NSs composite are calculated to be 2.01, 2.61, 1.86 and 2.32 eV, respectively. The prepared catalysts are efficiently utilized for the photocatalytic degradation of two neurotoxin compounds under UV and UV coupled with microwave irradiation. The prepared catalyst composites reveal excellent photocatalytic degradation of neurotoxin compound by degrading it up to 75% under UV and UV/microwave irradiation. The photocatalysis efficiency in UV/microwave system is higher than UV system. The result shows that the ZnO QDs/CuO NSs and TiO₂ QDs/WO₃ NSs composites have excellent photocorrosion inhibition and reusability properties. Thus, prepared samples with positive surface potential upon interaction with negative surface potential of *Enterococcus faecalis* and *Micrococcus luteus*.

1. Introduction

Water pollution is the contamination of water bodies (e.g. lakes, rivers, oceans, aquifers and groundwater). This form of environmental degradation occurs when pollutants are directly or indirectly discharged into water bodies without adequate treatment to remove harmful compounds [1,2]. MPTP (1-methyl-4-phenyl-1,2,3,6-tetrahydropyridine) is a prodrug to the neurotoxin MPP⁺, which causes rapid onset of Parkinsonism. MPTP as a lipophilic compound can cross the blood–brain barrier. Once inside the brain, MPTP is metabolized into the toxic cation 1-methyl-4-phenylpyridinium (MPP⁺) by enzymes. Tetanus toxin is an extremely potent neurotoxin and it's also called spasmogenic toxin, or TeNT. This toxin making it second only to Botulinum toxin (LD₅₀ 2 ng/kg) as the deadliest toxin in the world [3,4].

Photocatalysis is a science of employing catalyst that is utilized for speeding up chemical reactions that requires or engages light. A photocatalyst is defined as a material that is capable of absorbing light,

producing electron–hole pairs that enable chemical oxidation and reduction for transformations of the reaction participants and regenerate its chemical composition after each cycle of such interactions [5,6].

Tungsten oxide (WO₃) and copper oxide (CuO) is an n-type and p-type semiconductor which has low cost synthesis, non-toxicity, good thermal stability, photosensitivity, good electron transport properties [7,8].

Quantum dots (QDs) with narrow size distribution and high luminescent efficiency have attracted attention of researchers due to several properties. Recently, Titanium dioxide (TiO₂) and zinc oxide (ZnO) QDs are considered to be significant materials in the area of pollutant degradation due to their high photo catalytic efficiency. These materials are predominant semiconductor photocatalyst because of its stability, non-toxicity, low cost production and binding energy and band gap properties [9–18].

The main focus of the present investigation is to determine the photocatalytic performance of the synthesized products in degrading

* Corresponding author.

E-mail address: ali.fakhri88@yahoo.com (A. Fakhri).

TeNT and MPTP in UV and microwave irradiation and the antimicrobial activity for different microbes can be investigated.

2. Materials and Methods

2.1. Materials

All the chemicals were obtained from Sigma-Aldrich Ltd., USA.

2.2. Preparation of CuO Nanosheets and ZnO Quantum Dots Decorated CuO Nanosheets

In a typical synthesis process, 0.01 M aqueous solution (50 mL) of copper nitrate was mixed with 0.01 M aqueous solution of hexamethylenetetramine (50 mL) under vigorous stirring. In order to maintain a pH = 12 of the solution, KOH was added drop by drop with continuous stirring. After stirring, the suspension was transferred to Teflon-lined stainless steel autoclave and heated to 180 °C for 8 h. The product formed was filtered, washed with ethanol-water mixture solution and finally dried at 70 °C for 4 h in oven.

200 mg Zinc acetate and 500 mg of the as-prepared CuO nanosheets was added into 50 mL distilled water. The reaction was carried out by dropwise addition of KOH solution to zinc acetate solution with constant stirring. The final pH of the solution was maintained at 10. The obtained suspension was transferred into a 100-mL Teflon-lined stainless-steel autoclave, and then was heated to 180 °C for 10 h. After natural cooling to room temperature, the product was collected and washed with ethanol-water mixture solution.

2.3. Preparation of WO₃ Nanosheets and TiO₂ Quantum Dots Decorated WO₃ Nanosheets

10 mL of 65% nitric acid was dissolved in distilled water (40 mL) and stirred for 10 min. 1 g Na₂WO₄·2H₂O were dissolved homogeneously in 20 mL distilled water and were slowly added under continuous magnetic stirring. After stirring for another 30 min, the suspension was putted into a 100 mL Teflon-lined stainless-steel autoclave, sealed and heated to 180 °C for 3 h. Then, the product was centrifuged and washed with distilled water and ethanol several times. The sample was dried in vacuum at 60 °C for 12 h.

Initially 5.0 mL of TTIP and 500 mg WO₃ nanosheets was added into in 150 mL of isopropanol in a 500 mL beaker. Then, the mixed solution was stirred for more than 1 h. 0.01 mol of aqueous CTAB was added drop-wise into the mixed solution. The obtained suspension was transferred into a 100 mL Teflon-lined stainless-steel autoclave, and then was heated to 180 °C for 10 h. The finely ground sample was calcinated at 350 °C for 30 min.

2.4. Characterization Instruments

A Transmission Electron Microscope (TEM) (Zeiss EM-900) was used to examine the particle size and morphology of prepared samples and X-ray diffractometer (XRD) Philips X'Pert was measured for evaluation of crystalline information. X-ray photoelectron spectroscopy (Kratos Axis Ultra DLD) and UV-vis spectroscopy studies (TEC Avaspec 2048) were performed for evaluation of optical information. Infrared spectrum was recorded by Bruker Hyperion 3000 FTIR spectrometer. Absorption spectra were recorded on Cary 100 BIO UV-visible spectrophotometer. Zeta potential measurements of the dilute dispersions (0.1 mg mL⁻¹) of the various samples were performed with a Brookhaven NanoBrook Omni Instrument at 25 °C.

2.5. Photocatalytic Activity

In order to evaluate the photocatalytic efficiency of the prepared samples, photocatalytic measurements were done by dispersion was put

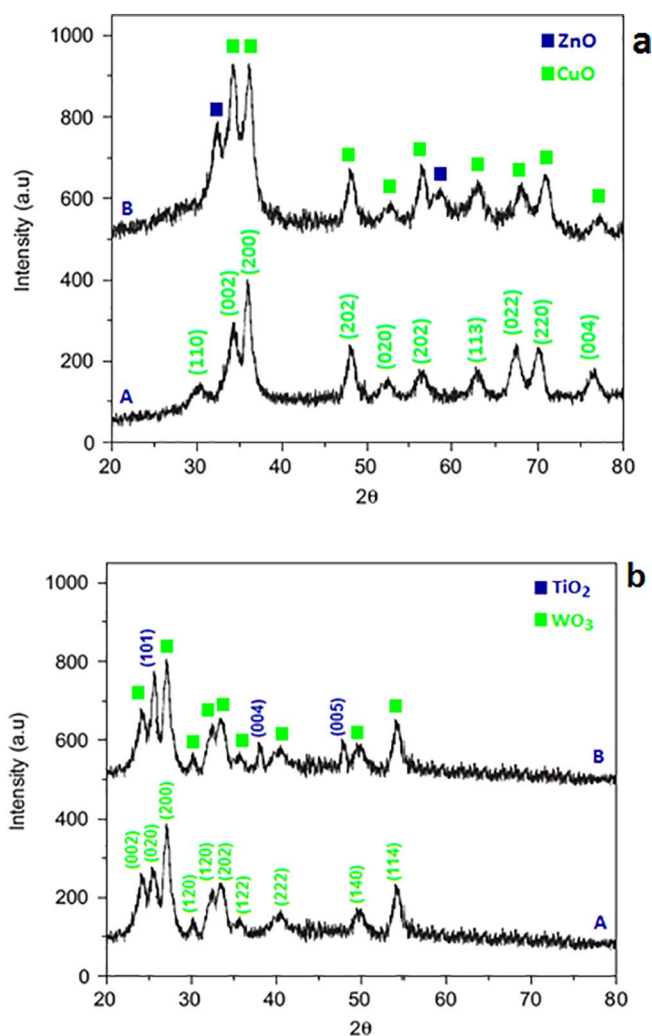


Fig. 1. XRD patterns of the prepared (a) CuO NSs (A) and ZnO QDs/CuO NSs (B), (b) WO₃ NSs (A) and TiO₂ QDs/WO₃ NSs (B).

in the side-arm glass cell with an optical length of 1 cm. After the glass cell was purged with Ar, it was placed into the ellipsoidal microwave applicator for irradiating the solution in the cell by microwaves. The temperature of the solution was kept by irradiating microwaves of 1.5 W. A spectroscopic cryostat was used to maintain the solution temperature. The sample was irradiated with a 300 W Xe lamp equipped with a UV mirror module ($\lambda < 400$ nm). For the measurement, a suspension of 10 mg of the as prepared photocatalyst powder and 100 mL of an aqueous solution of the TeNT and MPTP having a concentration of 1 mg/L were mixed and stirred in a dark place for about 30 min to reach the adsorption desorption equilibrium condition between the photocatalyst with TeNT and MPTP molecules. The TeNT and MPTP concentration was distinguished with the aid of a two dimensional Gas Chromatography (GC*GC) (Kimia Shangarf Pars Research CO., Iran). The column set used a first column 30 m \times 0.25 mm i.d. \times 0.25 μ m film thickness 5% phenyl-methyl siloxane phase serially coupled to a second column 1 m \times 0.1 mm i.d. \times 0.1 μ m film thickness 50% phenyl equivalent phase. Both columns which were temperature programmed from 70 to 320 °C. The injector temperature was 250 °C (injection volume of 1 mL) was employed in the split less mode. Helium was used as the carrier gas (2 mL/min).

2.6. Antibacterial Activity

The antibacterial activity was investigated by two bacterial strains, namely *Enterococcus faecalis* (gram positive) and *Micrococcus luteus*

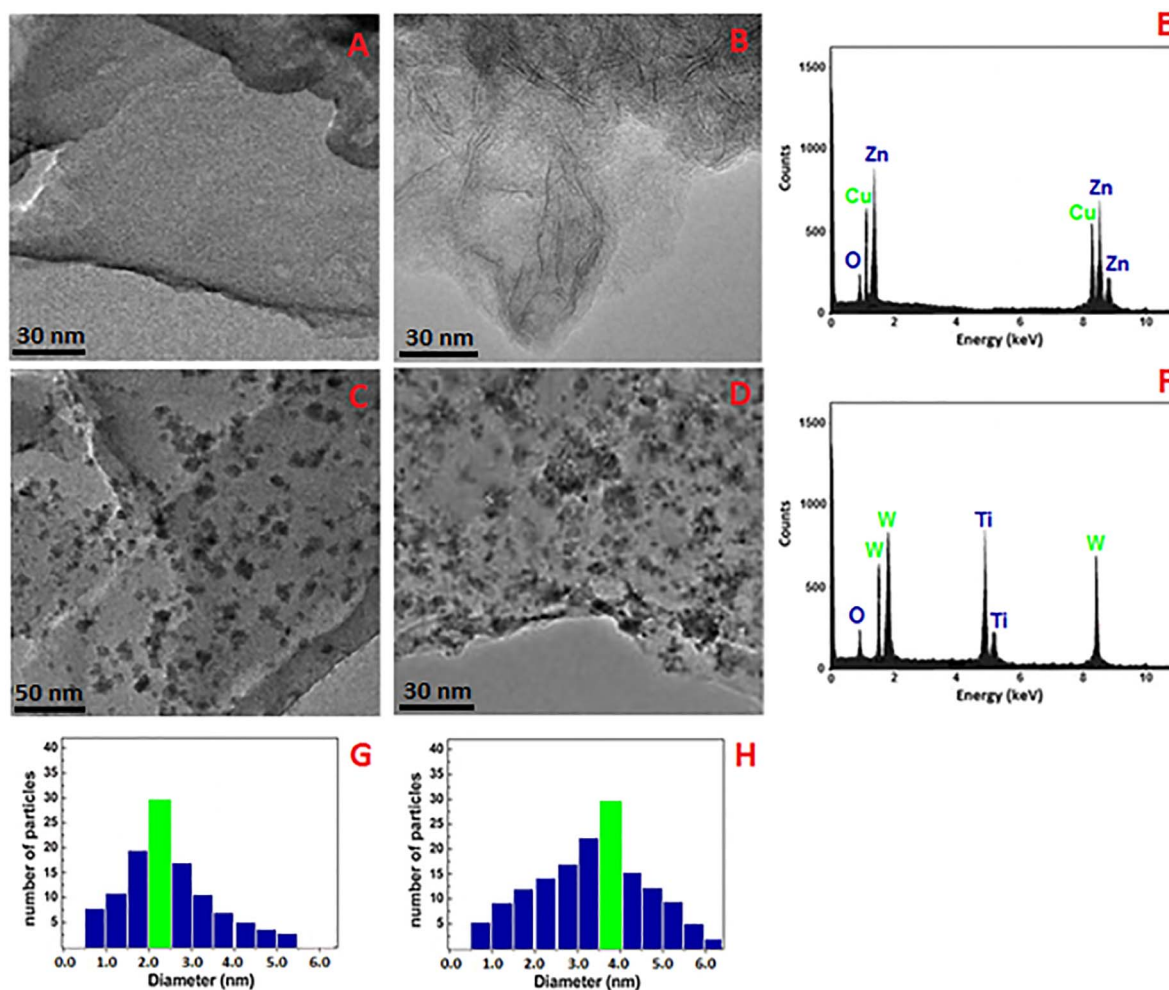


Fig. 2. TEM images of (A) CuO NSs, (B) WO₃ NSs, (C) ZnO QDs/CuO NSs, (D) TiO₂ QDs/WO₃ NSs; EDS spectra of (E) ZnO QDs/CuO NSs, (F) TiO₂ QDs/WO₃ NSs and particle size distribution histogram (G) ZnO QDs/CuO NSs, (H) TiO₂ QDs/WO₃ NSs.

(gram negative) microorganisms. In this experiment, the bacteria *E. faecalis* and *M. luteus* were cultivated by using the agar-disc-diffusion method. In this method, a nutrient agar medium (28 g/L in DI water) and nutrient broth (13 g/L in DI water) were prepared. The nutrient agar medium was then poured into autoclaved Petri dishes. The incubation was continued for 24 h at 37 °C, and after incubation, the zone of inhibition was analyzed to determine the antibacterial efficiency of the synthesized products.

2.7. Statistical Analysis

The data were expressed as the mean \pm the standard error of the mean ($n = 6$). Comparisons between the means of control and treated groups were made by one-way analysis of variance (using the statistical package Origin 6.1) with multiple comparison *t*-tests, and $p < 0.05$ is the limit of significance.

3. Results and Discussion

3.1. Characterization of the ZnO QDs/CuO NSs and TiO₂ QDs/WO₃ NSs

3.1.1. XRD

The XRD analysis was carried out to investigate the structure and crystal data of the as prepared samples. Fig. 1 depicts the XRD pattern of CuO NSs, WO₃ NSs, ZnO QDs/CuO NSs and TiO₂ QDs/WO₃ NSs composite. In the XRD spectra of the CuO NSs and WO₃ NSs, all the diffraction peaks are assigned according to the standard pattern of

monoclinic phase (JCPDS No: 05-0661 and JCPDS 43-1035), respectively. The diffraction peaks of ZnO QDs/CuO NSs are assigned to wurtzite phase for ZnO QDs structure (JCPDS No: 36-1451). Besides the representative peaks of the monoclinic phase of CuO NSs in the XRD spectra of the ZnO QDs/CuO NSs composite, we could not observe several peaks correspond to wurtzite phase for ZnO QDs. Fig. 1(a) clearly shows that there are several peaks in the diffraction pattern which reveals that as synthesized TiO₂ QDs are crystalline in nature. The Crystallite sizes were distinguished from the Scherrer equation [19–23] to be obtained 12.5, 13.25, 3.2 and 3.9 nm for CuO NSs, WO₃ NSs, ZnO QDs/CuO NSs and TiO₂ QDs/WO₃ NSs, respectively.

3.1.2. TEM

The structural morphology, shape, size and metal ration of the as prepared samples, as shown in Fig. 2. As can be seen, image confirms the sheet-like morphologies for the synthesized CuO and WO₃ nanosheets. Finally, Fig. 2C,D, which shows TEM images of the ZnO QDs/CuO NSs composite and TiO₂ QDs/WO₃ NSs, demonstrate that the ZnO QDs and TiO₂ QDs are well decorated over the CuO and WO₃ layers. Energy-dispersive X-ray spectroscopic analysis (Fig. 2E,F) indicates the presence of O, Zn, Cu, Ti and W elements in ZnO QDs/CuO NSs and TiO₂ QDs/WO₃ NSs, respectively. The average sizes of ZnO QDs/CuO NSs and TiO₂ QDs/WO₃ NSs (Fig. 2G&H) were found as 2.25, 3.75 nm, respectively.

3.1.3. X-ray Photoelectron Spectroscopy (XPS)

Quantitative spectroscopic method (X-ray photoelectron

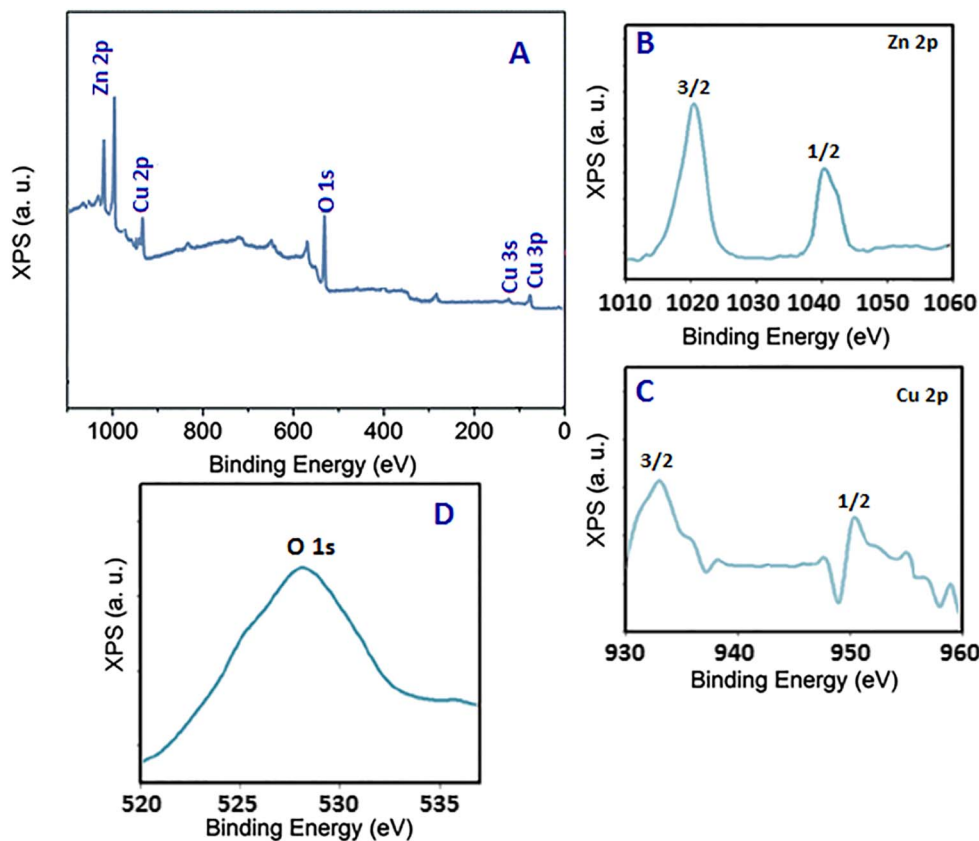


Fig. 3. The XPS spectra of survey spectrum for the ZnO QDs/CuO NSs composite (A), The fine spectra of Zn 2p (B), Cu 2p (C) and O 1s (D).

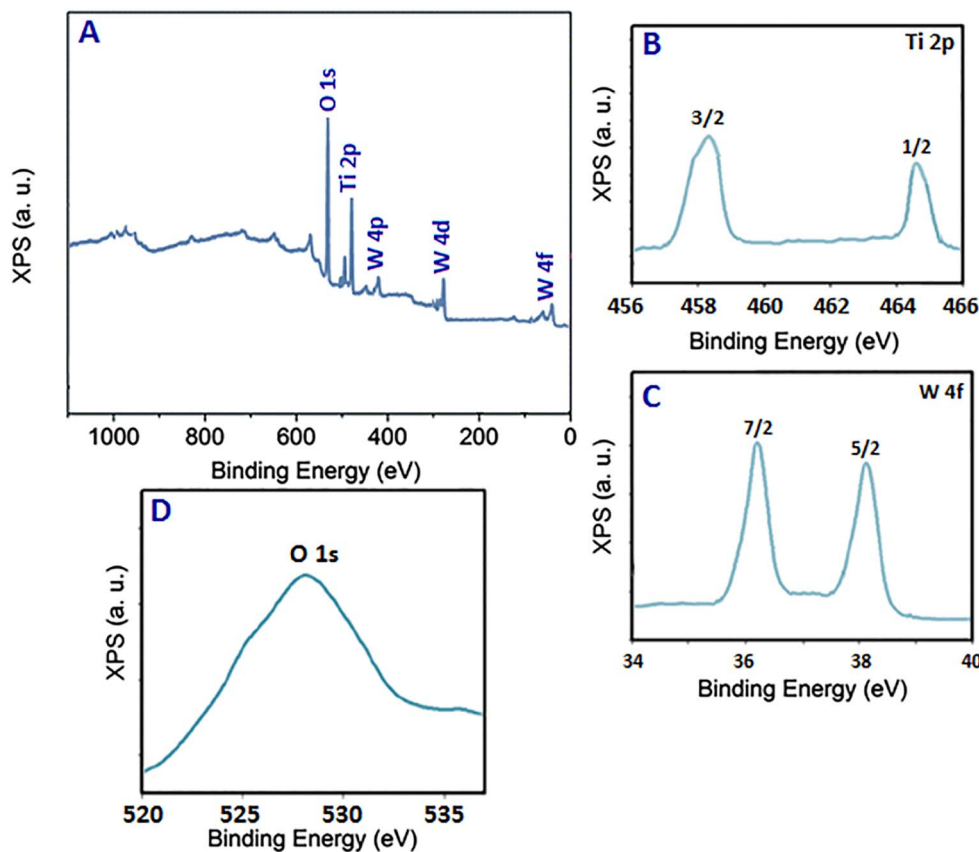


Fig. 4. The XPS spectra of survey spectrum for the TiO₂ QDs/WO₃ NSs composite (A), The fine spectra of Ti 2p (B), W 4f (C) and O 1s (D).

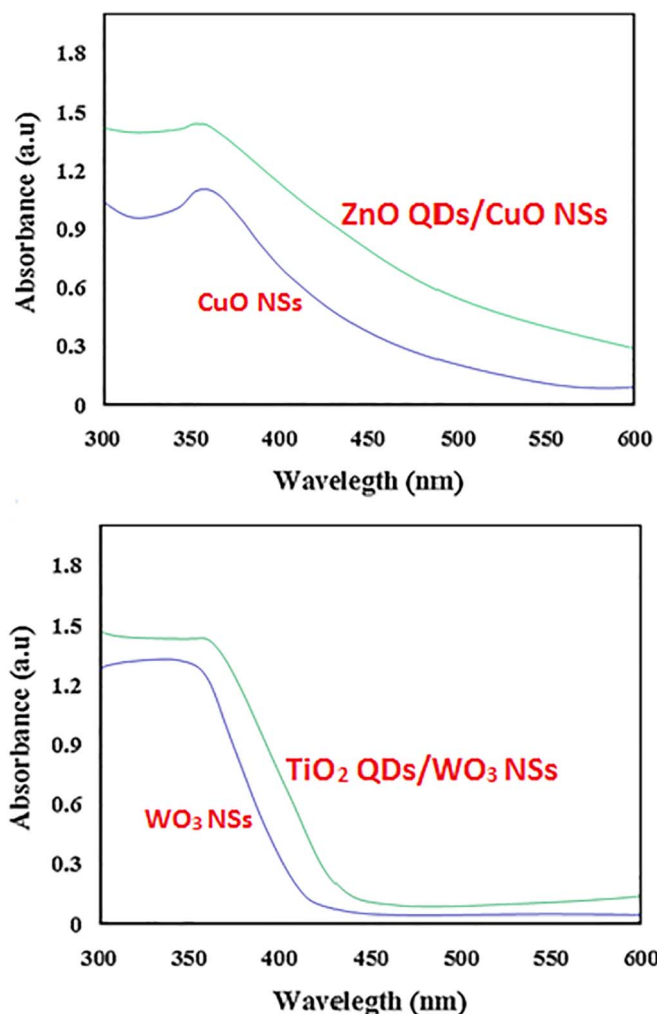


Fig. 5. UV–visible spectra of prepared samples.

spectroscopy) was used to determine the elemental analysis and the elements chemical states of the materials. The XPS spectra of Cu 2p, Zn 2p, and O 1s are displayed in Fig. 3A. From Fig. 3B, the spin orbit peaks of the Zn 2p_(3/2) and Zn 2p_(1/2) binding energy appeared at around 1020.0 eV and 1041.1 eV. From Fig. 3C, Cu 2p_(3/2) and Cu 2p_(1/2) binding energy appeared at around 931.5 eV and 951.1 eV. Fig. 3D indicated the O 1s spectrum at 528.0 eV is assigned to lattice oxygen (O₂[−]) for ZnO QDs/CuO NSs. The XPS spectra of Ti 2p, W 4f, and O 1s are displayed in Fig. 4A. From Fig. 4B, the spin orbit peaks of the Ti 2p_(3/2) and Ti 2p_(1/2) binding energy appeared at around 458.8 eV and 464.9 eV. From Fig. 4C, W 4f_(7/2) and W 4f_(5/2) binding energy appeared at around 36.5 eV and 38.2 eV. Fig. 4D indicated the O 1s spectrum at 528.0 eV is assigned to lattice oxygen (O₂[−]) for TiO₂ QDs/WO₃ NSs.

3.1.4. UV–vis Absorption Spectroscopy

Fig. 5 represents the UV–vis absorption spectra of the as-synthesized samples. These spectra are almost identical except for the slight variation in peak position and intensity of the absorbance band of the ZnO QDs/CuO NSs and TiO₂ QDs/WO₃ NSs composite. The absorption band edge of ZnO QDs/CuO NSs and TiO₂ QDs/WO₃ NSs composite is red-shifted compared to CuO NSs and WO₃ NSs, which may be due to the restoration network of the π - π conjugation of ZnO QDs and TiO₂ QDs in the composite [24]. The energy band gap (E_g) can be determined by using the following relation [25,26]:

$$(\alpha h\nu)^2 = A(h\nu - E_g)$$

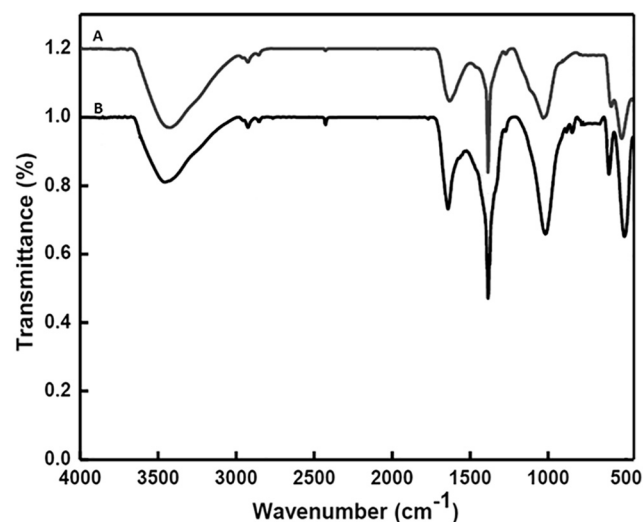


Fig. 6. FT-IR spectra of ZnO QDs/CuO NSs (A) and TiO₂ QDs/WO₃ NSs (B).

where α , $h\nu$, and A are the coefficient of absorbance, the energy of the incident photons, and a constant, respectively. The energy band gap of the CuO NSs and WO₃ NSs is calculated to be 2.01 and 2.61 eV whereas for the ZnO QDs/CuO NSs and TiO₂ QDs/WO₃ NSs composite a value of 1.86 and 2.32 eV is determined, respectively.

3.1.5. FTIR Spectroscopy

FTIR spectra were recorded in order to detect the formation of prepared catalyst. Fig. 6(A, B) represents the FT-IR spectra of synthesized ZnO QDs/CuO NSs and TiO₂ QDs/WO₃ NSs, respectively. The peaks at ~ 427 – 420 , ~ 528 – 511 and ~ 599 – 609 cm^{−1} correspond to the characteristic stretching vibration of metal-oxide bond in prepared catalyst. The bands around 1631–1641 cm^{−1}, 2923 cm^{−1} and 2854 cm^{−1} indicate the presence of –COO and –CH₂ group of capping agent.

3.2. Photocatalytic Activity

The photocatalytic performance of the as-synthesized samples is evaluated by the degradation of TeNT and MPTM under the UV light and UV coupled with microwave irradiation. The photocatalysis efficiency of the ZnO QDs/CuO NSs and TiO₂ QDs/WO₃ NSs composite was recorded as a function of irradiation time with a regular interval [27–32] and optimum time was found 60 min. Fig. 7 shows the photocatalysis

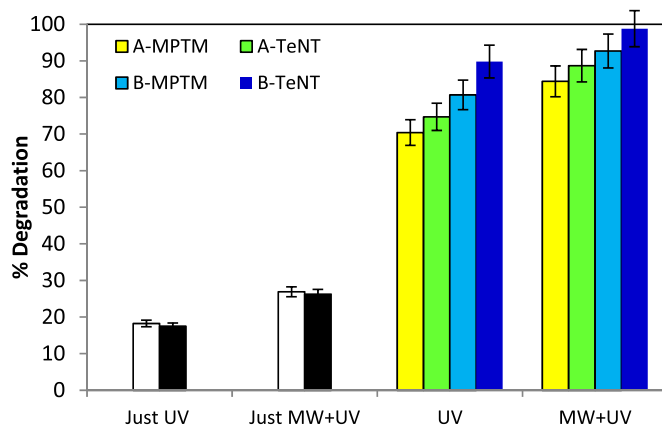


Fig. 7. Degradation efficiency of TeNT and MPTM by TiO₂ QDs/WO₃ NSs (A) and ZnO QDs/CuO NSs (B) under UV and microwave irradiation ($T = 25$ °C, catalyst dose: 10 mg, time: 60 min), (The black and white are related to degradation of TeNT and MPTM without any photocatalyst).

efficiency of UV/Microwave system is clearly higher than UV system. The microwave irradiation accelerates the photocatalytic degradation. Evidently, assistance of microwave is due to non-thermal effects of microwave such as polarization and dielectric properties. Specific interactions of the microwave radiation might give rise to the generation of additional surface defects that can directly increase the concentration of hydroxyl radicals species in the aqueous dispersion formation. The photogenerated electrons are produced O_2^- . The O_2^- superoxide and OH radicals act as strong oxidizing agents, which decomposing TeNT and MPTP. In the process of photodegradation, the absorption of photons by the ZnO QDs/CuO NSs and TiO_2 QDs/ WO_3 NSs composite with UV light/microwave results in holes in the valence band and a transfer of electrons into the energy states lying below the conduction band.

3.3. Photocorrosion Inhibition of Catalyst

To evaluate the photostability of the catalyst, the recycled experiments for the photodegradation of TeNT and MPTP were performed, and the results are shown in Fig. 8. The large amount of TeNT and MPTP could be degraded when ZnO QDs/CuO NSs and TiO_2 QDs/ WO_3 NSs was used for the first time, however, after three recycles, a slight decrease of photocatalytic activity for ZnO QDs/CuO NSs and TiO_2 QDs/ WO_3 NSs was found (Fig. 8) within 60 min. After exposure under UV light for 20 h, there was no change photocatalytic activity of ZnO QDs/CuO NSs and TiO_2 QDs/ WO_3 NSs for the TeNT and MPTP photodegradation. The drastic decrease of photocatalytic activity for CuO NSs and WO_3 NSs was resulted from the photocorrosion effect. This result strongly confirms the suppressed photocorrosion offered by the ZnO QDs and TiO_2 QDs, which effectively inhibit photocorrosion.

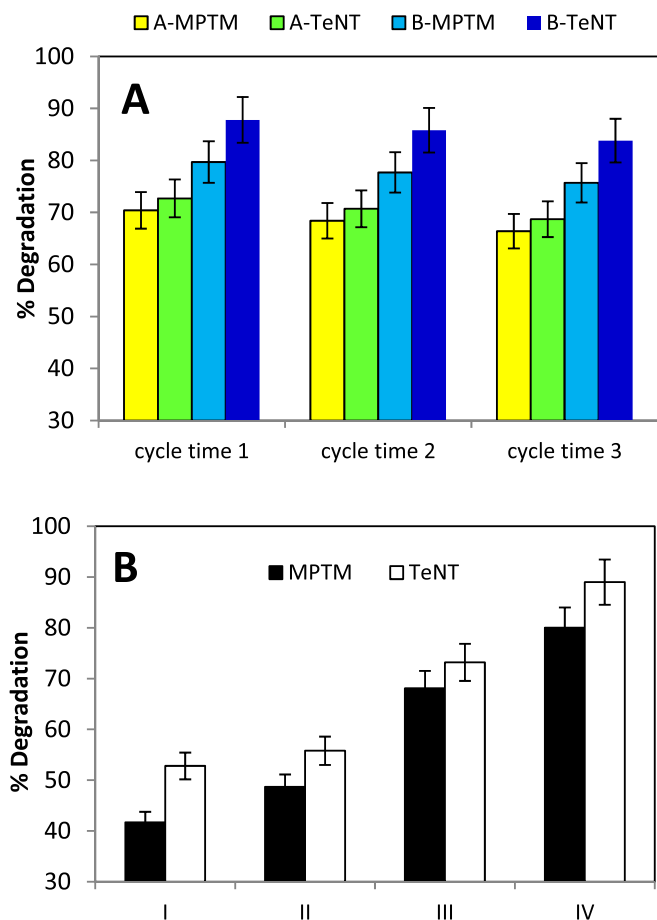


Fig. 8. Photostability graphs of prepared catalyst (A) under irradiation with UV light in three cycle runs (A: TiO_2 QDs/ WO_3 NSs, B: ZnO QDs/CuO NSs); (B) under irradiation with 20 h UV light (I: WO_3 NSs, II: CuO NSs, III: TiO_2 QDs/ WO_3 NSs, IV: ZnO QDs/CuO NSs).

3.4. Reusability

Reusability of the catalyst is one of the most projected attractions of any heterogeneous catalyzed reaction. Regeneration of the catalyst, ZnO QDs/CuO NSs and TiO_2 QDs/ WO_3 NSs, was done after each reaction, by centrifugation, washing with water, and further treatment at the calcination temperature of the catalyst, that is, at 200 °C, for 1 h. The photocatalytic activity of the prepared catalyst remains intact even up to ten consecutive experiments under the selected reaction conditions (Figure not shown). The performance of the ZnO QDs/CuO NSs and TiO_2 QDs/ WO_3 NSs in the degradation of a toxin pollutants was also tested where the activity is found to be admirable.

3.5. Antibacterial Activity

We have also studied the antibacterial activity of the ZnO QDs/CuO NSs, TiO_2 QDs/ WO_3 NSs. The measurements were performed on *E. faecalis* (gram positive) and *M. luteus* (gram negative) bacterial strains as zone of inhibition tests. The antibacterial activity of the ZnO QDs/CuO NSs, TiO_2 QDs/ WO_3 NSs was investigated (Figure not shown). Fig. 9 shows the zeta potential value of bacteria and ZnO QDs/CuO NSs and TiO_2 QDs/ WO_3 NSs used in the study. Negative and positive zeta potential values are obtained for bacteria and prepared catalyst, respectively. A possible explanation for the anti-microbial activity of the metal oxide nanostructures against the *E. faecalis* and *M. luteus* bacterial strains is an electrostatic interaction between the positive metal oxide nanostructures and the negative charges of the microbes [33–35], which prevent the further growth of the microbes. From the results, it is evident that lower concentrations of samples do not show significant effect on growth kinetics of the bacteria. However, 100 μ g/mL of samples in culture exerts significant growth inhibition for *E. faecalis* and *M. luteus*. It was found that the MIC values for the antibacterial assay in the presence of nanomaterials as shown in Table 1.

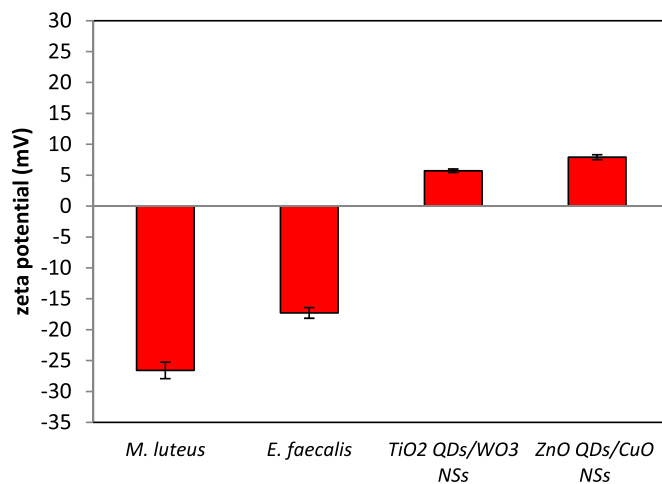


Fig. 9. The zeta potential of all samples.

Table 1
Zone of inhibition (mm) of ZnO QDs/CuO NSs, TiO_2 QDs/ WO_3 NSs against antibacterial.

| Bacterial | Zone of inhibition (mm) | | |
|--------------------|-------------------------|-------------------------|-------------|
| | ZnO QDs/CuO NSs | TiO_2 QDs/ WO_3 NSs | Control |
| <i>E. faecalis</i> | 14.23 ± 0.31 | 13.41 ± 0.41 | 3.81 ± 0.25 |
| <i>M. luteus</i> | 12.11 ± 0.27 | 11.27 ± 0.37 | 3.01 ± 0.13 |

4. Conclusions

We have performed a synthesis of all catalyst via a hydrothermal method. The synthesized samples were characterized by XRD, TEM, XPS, FTIR, EDS and UV–vis spectroscopy. TEM measurements confirmed the ZnO and TiO₂ QDs dispersed over CuO and WO₃ NSs. The decrease in the value of the optical band gap calculated using UV–vis data of the ZnO QDs/CuO NSs and TiO₂ QDs/WO₃ NSs composite compared to CuO NSs and WO₃ NSs may be due to the interaction between quantum dots and nanosheets. The ZnO QDs/CuO NSs and TiO₂ QDs/WO₃ NSs are successfully applied for the photocatalytic degradation of TeNT and MPTP under UV and UV/microwave irradiation. In summary, the ZnO QDs/CuO NSs and TiO₂ QDs/WO₃ NSs show considerable potential for an application as photocatalytic and anti-bacterial material.

Acknowledgment

The authors gratefully acknowledge supporting of this research by the Young Researchers and Elites club, Islamic Azad University, Science and Research Branch.

References

- [1] H. Tong, S. Ouyang, Y. Bi, N. Umezawa, M. Oshikiri, J. Ye, Nano-photocatalytic materials: possibilities and challenges, *Adv. Mater.* 24 (2012) 229–251.
- [2] R. Abe, Recent progress on photocatalytic and photoelectrochemical water splitting under visible light irradiation, *J. Photochem. Photobiol. C* 11 (2010) 179–209.
- [3] World Health Organization (Ed.), *Botulism*, 2017 (Retrieved 2017-01-18).
- [4] A.K. Verma, R.R. Das, P. Bhunia, A review on chemical coagulation/flocculation technologies for removal of colour from textile waste waters, *J. Environ. Manag.* 93 (2012) 154–168.
- [5] M. Mehrjouei, S. Muller, D. Moller, A review on photocatalytic ozonation used for the treatment of water and waste water, *Chem. Eng. J.* 263 (2015) 209–219.
- [6] J. Xiao, Y. Xie, H. Cao, Organic pollutants removal in waste water by heterogeneous photocatalytic ozonation, *Chemosphere* 1 (2015) 1–17.
- [7] S. Steinhauer, E. Brunet, T. Maier, G.C. Mutinati, A. Köck, O. Freudenberg, C. Gspan, W. Grogger, A. Neuhold, R. Resel, Gas sensing properties of novel CuO nanowire devices, *Sensors Actuators B Chem.* 187 (2013) 50–57.
- [8] A. Klinbumrung, T. Thongtem, S. Thongtem, Characterization and gas sensing properties of CuO synthesized by DC directly applying voltage, *Appl. Surf. Sci.* 313 (2014) 640–646.
- [9] J. Joo, S.G. Kwon, J.H. Yu, T. Hyeon, *Adv. Mater.* 17 (2005) 1873.
- [10] F. Qu, D.R. Santos, N.O. Dantas, A.F.G. Monte, P.C. Morais, *Phys. E* 23 (2004) 410.
- [11] K.-F. Lin, H.-M. Cheng, H.-C. Hsu, L.-J. Lin, W.-F. Hsieh, *Chem. Phys. Lett.* 409 (2005) 208.
- [12] A. Ivask, K.G. Scheckel, P. Kapruwan, V. Stone, H. Yin, N.H. Voelcker, E. Lombi, *Nanotoxicology* 11 (2017) 150–156.
- [13] Attarad Ali, Sidra Ambreen, Qaisar Maqbool, Sania Nazk, Muhammad Fahad Shams, Madiha Ahmad, Abdul Rehman Phulle, Muhammad Zia, *J. Phys. Chem. Solids* 98 (2016) 174–182.
- [14] Yu-Huei Peng, Yi-Chun Tsai, Chia-En Hsiung, Yi-Hsuan Lin, Yang-hsin Shih, *J. Hazard. Mater.* 322 (2017) 348–356.
- [15] A. Ali, S. Ambreen, R. Javed, S. Tabassum, I. Ul Haq, M. Zia, *Mater. Sci. Eng. C* 74 (2017) 137–145.
- [16] Mohsen Mansouri, Mohsen Nademi, Mohammad Ebrahim Olya, Hossein Lotfi, *Journal of Chemical Health Risks* 7 (2017) 19–32.
- [17] Tropita Piplai, Arun Kumar, Babu J. Alappat, *Water Sci. Technol.* 75 (2017) 928–943.
- [18] Rabia Javed, Madiha Ahmed, Ihsan Ul Haq, Sobia Nisa, Muhammad Zia, *Mater. Sci. Eng. C* 79 (2017) 108–115.
- [19] Ali Fakhri, Mona Azad, Shiva Tahami, *J. Mater. Sci. Mater. Electron.* 28 (2017) 16397–16402.
- [20] Ali Fakhri, Sajjad Behrouz, *Sol. Energy* 117 (2015) 187–191.
- [21] Ali Fakhri, Sajjad Behrouz, *Sol. Energy* 112 (2015) 163–168.
- [22] M.E. Borges, M. Sierra, E. Cuevas, R.D. García, P. Esparza, *Sol. Energy* 135 (2016) 527–535.
- [23] Ganesh B. Markad, Sudhir Kapoor, Santosh K. Haram, Pragati Thakur, *Sol. Energy* 144 (2017) 127–133.
- [24] A. Fakhri, P. Afshar Nejad, M. Pourmand, *J. Photochem. Photobiol. B* 159 (2016) 211.
- [25] A. Fakhri, S. Behrouz, M. Pourmand, *J. Photochem. Photobiol. B* 149 (2015) 45.
- [26] A. Fakhri, R. Khakpour, *J. Lumin.* 160 (2015) 233–237.
- [27] A. Fakhri, M. Pourmand, R. Khakpour, S. Behrouz, *J. Photochem. Photobiol. B* 149 (2015) 78.
- [28] D. Lu, P. Fang, X. Liu, S. Zhai, C. Li, X. Zhao, J. Ding, R. Xiong, *Appl. Catal., B* 179 (2015) 558–573.
- [29] D. Lu, B. Zhao, P. Fang, S. Zhai, D. Li, Z. Chen, W. Wu, W. Chai, Y. Wu, N. Qi, *Appl. Surf. Sci.* 359 (2015) 435–448.
- [30] D. Lu, P. Fang, Y. Liu, Z. Liu, X. Liu, Y. Gao, F. Chen, F. Niu, *J. Nanopart. Res.* 16 (2014) 1–12.
- [31] D. Hazarika, N. Karak, Photocatalytic degradation of organic contaminants under solar light using carbon dot/titanium dioxide nanohybrid, obtained through a facile approach, *Appl. Surf. Sci.* 376 (2016) 276–285.
- [32] A. Qu, H. Xie, X. Xu, Y. Zhang, S. Wen, Y. Cui, *Appl. Surf. Sci.* 375 (2016) 230–241.
- [33] V. Lakshmi Prasanna, Rajagopalan Vijayaraghavan, *Mater. Sci. Eng. C* 77 (2017) 1027–1034.
- [34] Yanhui Hou, Jiantao Feng, Ye Chen Wang, Liangchao Li, *J. Mater. Sci. Mater. Electron.* 27 (2016) 6615–6622.
- [35] S. Ramya, G. Viruthagiri, R. Gobi, N. Shanmugam, N. Kannadasan, *J. Mater. Sci. Mater. Electron.* 27 (2016) 2701–2711.